A model to optimize the selectivity of gas separation in membranes

Zachary D. Pozun [a,b], Graeme Henkelman [a,b,*]

[a] Department of Chemistry and Biochemistry, 1 University Station A5300, The University of Texas at Austin, Austin, TX 78712-0165, USA
[b] Institute for Computational Engineering and Sciences, 1 University Station CO200, The University of Texas at Austin, Austin, TX 78712-0165, USA

ARTICLE INFO

ABSTRACT

We present a model of olefin/paraffin separation via nanocomposite membranes and a corresponding lattice kinetic Monte Carlo simulation. Our model is based on the solution-diffusion theory of facilitated transport through microporous membranes and the preferential binding of olefins to silver ions and nanoparticles. In our model, olefin molecules bind to the randomly distributed traps on a lattice whereas paraffin molecules do not. Selectivity for olefins over paraffins in the steady state is explained in terms of lattice diffusion and the equilibrium statistics of adsorbed gases. We show that, to first order, the maximum selectivity occurs when the rate at which an olefin molecule enters the lattice is the same as rate at which it leaves a trap site. The maximum selectivity is higher for weaker binding traps than for strong binding traps. Our model also demonstrates that the maximum selectivity increases with nanoparticle loading in the membrane and that, when the selectivity is maximized as a function of olefin binding and applied pressure, the olefin permeability is reduced from the neat membrane by a constant factor.

1. Introduction

Every year approximately 150 million tons of light olefins – ethylene and propylene – are produced in the petrochemical industry at great energetic cost [1]. Approximately 1.4×10^{14} BTUs per year are invested to separate ethane from ethylene and propane from propylene [2]. The boiling points of ethylene, 169 K, and ethane, 184 K [3] are close enough that large cryodistillation fractionating columns are required for efficient separation.

The separation is energy intensive in large part due to the phase change. The light olefin mixtures are cooled under high pressure before fractionation. Membrane separation of gases, in contrast, does not require a phase change. A stable membrane for olefin/paraffin separation would lead to significant energy savings and lower costs during industrial production of ethylene and propylene. Designing a robust and highly olefin selective membrane, however, remains an open problem.

Models of gas separation membranes are commonly based on the mechanism of separation. Models of gas permeation treat the membrane as a porous network of polymer chains containing microcavities of diameters ranging from 5 to 1000 Å. Solution-diffusion membranes, in which transient gaps appear due to thermal motion, stand in contrast to rigid polymers that act as molecular sieves [5]. In the limit of large microcavities in the pore-flow model, permeation is a pressure-driven process of gas flow through small pores in which large molecules are separated from smaller molecules based on size.

In the limit of small microcavities on the order of 5–10 Å, however, permeation becomes a diffusive process controlled by the thermal motion of the constituent membrane polymers [4]. Permeation in this limit consists of three distinct steps [6]:

1. Adsorption at the upstream face.
2. Diffusion through the membrane based on thermal motion of polymer chains.
3. Desorption from the downstream face.

Step 2 has been modeled using molecular dynamic (MD) simulations of gas molecules in membrane cavities [7–10]. Particles move from cavity to cavity based on the thermal fluctuations of membrane polymers. Lim and Tsotsis [11] performed MD simulations of CO_2 and CH_4 permeation in polyetherimide matrices and observed that molecular displacement over time from initial positions are marked by small displacements within a microcavity punctuated with much larger rapid displacements corresponding to a hop to a nearby microcavity. The ability to hop between cavities is controlled by thermal motion that opens temporary channels between cavities and results in diffusion-controlled permeation.

The overall diffusion constant for a gas molecule in a specific membrane, as predicted by the solution-diffusion model, is

* Corresponding author at: Department of Chemistry and Biochemistry, 1 University Station CO200, The University of Texas at Austin, Austin, TX 78712-0165, USA. Tel.: +1 512 471 4179.
E-mail address: henkelman@mail.utexas.edu (G. Henkelman).

a function of temperature and its own cross-sectional area. Smaller molecules pass more easily through thermally opened channels between microcavities. In the olefin/paraffin separation problem, olefins have a smaller cross sectional area than the corresponding paraffin. Experimental results, as predicted, demonstrate that neat organic membranes commonly have a large selectivity for olefins over the corresponding paraffin [3,12,13].

There is a tradeoff, however, between permeability and selectivity. Burns and Koros [14] report an experimentally observed upper bound to propylene/propane selectivity as a function of propylene permeability. The greatest selectivity is observed at low propylene permeability, whereas selectivity falls to unity at very high propylene permeabilities. An industrially desirable membrane, in contrast, maximizes both permeability and selectivity in order to achieve efficient selectivity in the shortest amount of time and the least amount of membrane. Facilitated transport membranes have been demonstrated to increase both selectivity and permeability and offer strong promise for industrial separations [15].

Membranes containing ionic silver complexed with a counterion, such as BF_4^-, and supported in an organic polymer scaffold have been demonstrated to have a high selectivity for olefins over paraffins in the equilibrium gas flux [16–20]. The silver ions selectively bind to olefins through a d–π^* complexation that is unavailable to paraffins, which contain only σ bonds in the carbon backbone [15]. The silver–olefin complex is particularly unstable upon exposure to air, however, which is undesirable for industrial applications [21].

Membranes that replace ionic silver with silver nanoparticles provide an appealing alternative for olefin/paraffin separation [22–24]. Membranes containing silver nanoparticles have been demonstrated to be much more stable for olefin/paraffin separation over time [25].

Methods such as laser ablation of microparticles (LAM) are capable of producing small, relatively monodisperse nanoparticles without surfactants [26,27]. LAM may be used to generate core/shell nanoparticles of metal/metal as well as metal/metal oxide [28,29]. Core/shell nanoparticles are of particular interest due to their tunable properties by varying the composition and thickness of the core and shell independently [30–32].

In this work, we present a model of membrane separation for membranes containing olefin-binding nanoparticles. We seek to predict overall trends in selectivity as a function of the olefin binding energy to nanoparticles. Changes in the selectivity as a function of pressure is explained in terms of changes to the sorption and diffusivity of the component molecules.

2. Model details

Beginning with the solution-diffusion model, five macroscopic parameters are required to model a gas separation membrane that contains nanoparticles. The diffusivity of molecules in the neat membrane provides hopping rates for large diffusive jumps between lattice sites. The density of nanoparticles in the membrane and the olefin–nanoparticle binding energy to give an Arrhenius probability of finding the olefin molecule bound to a nanoparticle. The upstream pressure and the sorption coefficient provide the concentration of gas molecules along the upstream edge of the membrane in steady state.

In the solution-diffusion model, the membrane is treated as a series of microcavities that gas molecules hop between based on the thermal motion of the membrane's polymer chains. This behavior as represented in a lattice kinetic Monte Carlo (KMC) model as molecules that may hop to adjacent sites on a $N \times N$ grid. A single lattice site may only be occupied by a single gas molecule.
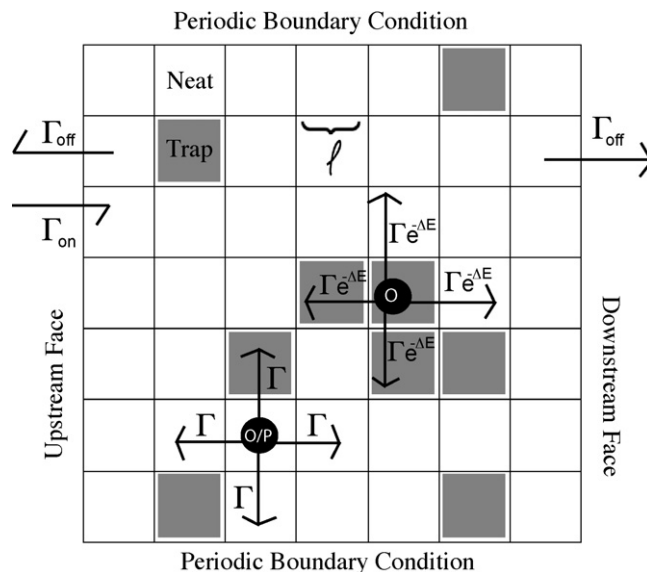

Fig. 1. Parameters for the KMC model are shown on a small, sample lattice. The olefin hopping rate from a trap is $\Gamma \exp(-\Delta E)$; paraffin hopping rates from traps are the same as neat sites, Γ.

Periodic boundary conditions are applied at two opposite lattice edges. Molecules that diffuse across the edge are brought back in the corresponding row at the opposite edge. Similarly, molecules at one of the edges can be blocked by a molecule in the same row at the opposite edge. The lattice size is chosen such that edge effects do not appear. In this manner, an effectively infinitely long slice through a membrane is simulated.

The diffusivity, D, of the gas in the membrane provides the site-to-site hopping rate for gas molecules in the membrane. For a membrane with diffusivity, D, the rate of site-to-site hopping, Γ, is given by

$$D = \Gamma \ell^2, \tag{1}$$

where ℓ is the diffusional jump distance. Eq. (1) is closely related to the Einstein–Smoluchowski relation; however, in the KMC model Γ represents the hopping rate to a single given adjacent site, not to any of the four adjacent sites as in the case of surface diffusion. The value of ℓ for a membrane of total thickness L is given by $L = \ell N$. In the KMC model, ℓ is the natural unit of length and varying it while holding the number of lattice points, N, constant represents a change to the diffusional jump length. In what follows, ℓ is taken to be the unit of length.

Fig. 1 shows how the membrane is modeled with KMC. An olefin/paraffin gas mixture reversibly adsorbs to the membrane along one face, diffuses through the membrane, and passes through the downstream face to be collected in a vacuum. In order to simulate the behavior of membranes containing olefin-specific binding agents, randomly distributed lattice sites are treated as traps. The fraction of trap sites, ρ, is a fixed parameter. Olefins on the lattice bind to the traps with a binding energy, ΔE. The paraffin molecules, however, do not bind to the trap sites and, thus, behave as if every lattice site were a neat membrane site.

From a neat membrane site, the hopping rate, Γ, is the rate for a molecule to hop to an adjacent, unfilled site. The hopping rate from a trap site for olefin molecules becomes $\Gamma \exp(-\Delta E)$ and remains Γ for paraffin molecules. The binding energy ΔE is expressed in units of $k_B T$ so that it appears as a unitless quantity in the Arrhenius expression.

The choice of N is dictated by the sorption coefficient, S, which relates the concentration of molecules at the upstream face of the

membrane, C, at an applied pressure, p, by

$$S = \frac{C}{p}. \tag{2}$$

For a membrane of fixed thickness, L, and applied pressure, increasing N increases the number of gas molecules adsorbed along the upstream edge. Membranes with a large sorption coefficient necessitate a finer lattice.

The last macroscopic parameter is the applied pressure at the upstream face. The parameters of the simulation are in terms of kinetic rates, however, not macroscopic pressures. A gas at pressure p in equilibrium with a surface containing adsorption sites forms a Langmuir isotherm,

$$\theta(p) = \frac{p}{1 + p}, \tag{3}$$

where p is taken to be in reduced units of the pressure, p_0, at which half of the sites are occupied. In this way, the pressure is a unitless quantity defined by the sorption isotherm of the physical membrane. The pressure is related to the rates of hopping onto and off of the surface in the KMC model by

$$p = \frac{\Gamma_{on}}{\Gamma_{off}}. \tag{4}$$

The rate of desorption from the surface, Γ_{off}, is chosen to be equal to the rate of hopping between sites in the membrane, Γ. Then, the pressure determines the rate for a molecule to hop onto the membrane on the upstream face Γ_{on} in the KMC model.

We have chosen to model separations for an upstream gas containing equal partial pressures of olefin and paraffin. In the KMC model, this is established with an equal probability for these molecules to hop onto the lattice. The concentration of the individual gas components along the leading edge is given in terms of the partial pressures by $\frac{1}{2}\theta(p)$.

Opposite the upstream face of the membrane is the downstream face. On this edge, molecules may leave the lattice with rate Γ_{off}. Vacuum is enforced by setting the rate of molecules re-entering along the downstream face to zero. Molecules leaving along this edge are counted in the output flux of gas through the membrane.

A standard KMC algorithm is employed to model the diffusion of particles along the lattice. Initial conditions are implemented by randomly distributing trap sites in the membrane based on ρ. With each KMC step, a cumulative function, R, is generated consisting of the sum of all rates available to the system in the current state. A random number is chosen on $[0, R]$. A given process is then selected from R such that processes are proportionately weighted so that faster processes are selected proportionately faster than slower processes. A second random number, u, is generated on $(0, 1]$ and the time step is updated as

$$\Delta t = \frac{-\ln u}{R}. \tag{5}$$

The unit of time in our model is taken to be Γ^{-1}. The selected process is then carried out and R is updated to reflect any processes that either became available or unavailable in the new state, where the algorithm is repeated. For a detailed description of the KMC method, refer to Voter [33].

3. Results and discussion

The motivation for this work is to identify the statistical basis of selectivity for olefins over paraffins in the steady state in gas separation nanocomposite membranes. To accomplish this goal, the equations for the flux of each component gas are derived for both the neat and trap-containing membranes. While the concentration of each gas along the front edge is given exactly by the Langmuir
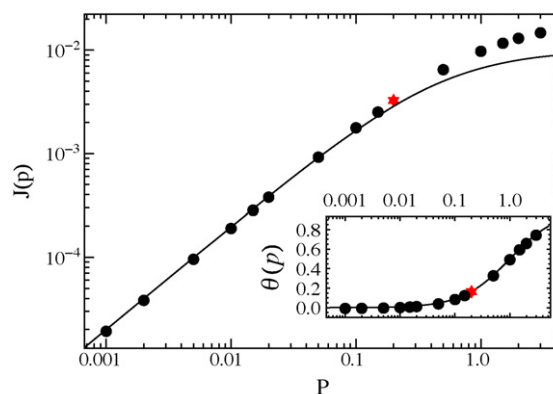
Fig. 2. The flux of particles in a neat membrane is plotted as a function of temperature. Inset is the Langmuir isotherm also as a function of pressure. The solid lines are analytical predictions of Eqs. (3) and (7), and solid black circles are time-averaged concentrations from individual KMC simulations. The red star marks the data point at which KMC simulations begin to diverge. (For interpretation of the references to colour in this figure legend, the reader is referred to the web version of the article.)

isotherm, the diffusion statistics of the gases on the lattice are not known exactly. With the flux equations derived, the statistical basis for selectivity is an optimization problem in three parameters – p, ΔE, and ρ – that can be solved analytically by separating the problem into the following components.

3.1. Flux through a neat membrane

The permeability, P, of a single gas component in a membrane is defined as the product of the diffusivity, D, and the sorption, S, in the membrane. The permeability is a material property given by

$$P = SD = \frac{JL}{\Delta p}, \tag{6}$$

where Δp is the applied pressure difference and J is the flux of gas through the membrane. In the KMC model, a vacuum is present at the downstream face, so that the applied pressure across the membrane is the same as the upstream pressure, $\Delta p = p$.

As defined in Eq. (2), the sorption, S, is the concentration of gas along the upstream face of the membrane divided by the applied pressure. Within the KMC model, the concentration of gas molecules along the edge of the lattice follows the Langmuir adsorption isotherm in Eq. (3). KMC simulations were performed on a neat membrane and the time-averaged concentration of molecules along the edge in equilibrium with the gas are shown (inset in Fig. 2) to agree with the Langmuir isotherm.

An expression for the flux through a single lattice site on the downstream face is derived by substituting KMC model parameters into Eq. (6) of the membrane to obtain

$$J = \Gamma \frac{\theta(p)}{L}. \tag{7}$$

The flux of particles through the unit length ℓ in unit time Γ^{-1} at the downstream face is a function of p and the thickness L. As shown in Fig. 2, there is good agreement between the KMC data and Eq. (7) in the tracer diffusion limit, where the value of $\theta(p)$ is very close to zero and all molecules follow a two-dimensional random walk. As shown by the red star, when the front edge of the lattice begins to fill, the KMC flux diverges from Eq. (7). This expression assumes a vacuum at the downstream face. A non-zero back pressure would contribute a correction term from Eq. (3) that is not significant in the linear-flux regime.

Along the axis between the upstream and downstream faces, the diffusion of molecules is mathematically analogous to the problem of the random walk in one dimension with an absorbing boundary.
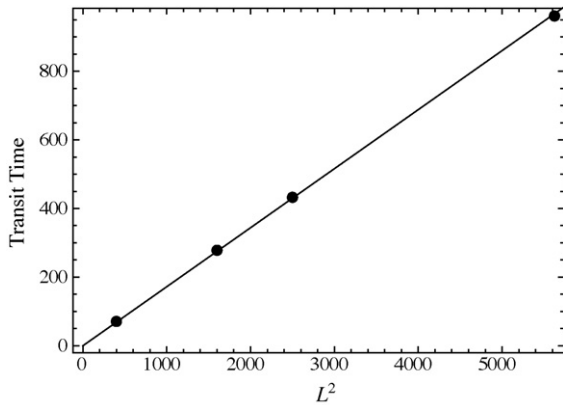
Fig. 3. The average transit times for molecules that enter the membrane at the upstream face and eventually reach the downstream face are plotted as a function of L^2. Individual dots are KMC data points and the line is a linear fit.

For a semi-infinite line $(x \geq 0)$ with an absorbing barrier at the origin and the tracer initially at x_0 along the line, the probability of first hitting $x = 0$ at time t is derived by Chandrasekhar [34] as

$$f(t) = \frac{x_0}{\sqrt{4\pi D t^3}} \exp\left(\frac{-x_0^2}{4Dt}\right). \qquad (8)$$

The mean first passage time to reach $x = 0$,

$$\langle t \rangle = \int_0^\infty t f(t)dt = \infty, \qquad (9)$$

does not converge due to the fraction of tracers that spend most of their time at large x before returning to $x = 0$. Without the fat tail, the typical diffusion time over the distance x_0 scales like

$$t_{x0} \sim \frac{x_0^2}{4D}. \qquad (10)$$

On the membrane, however, molecules that move in the opposite direction simply hop off of the membrane into the source gas. Eq. (10) provides an approximate scaling law for the average transit time for a molecule diffusing between the upstream and downstream face.

In Fig. 3 the observed transit times from the KMC model are plotted as a function of membrane thickness, L. With increasing thickness, the transit times are linear with L^2. The least-squares fit of a trend line passing through the origin gives a slope of $\frac{0.688}{4D}$, which is consistent with the prediction from Eq. (10).

### 3.2. Membranes containing traps

In the KMC model, paraffin molecules see no change in hopping rate from any site, whereas olefin molecules hop at either Γ from a neat site or $\Gamma \exp(-\Delta E)$ from a trap site due to the binding energy ΔE. The overall effect of the heterogeneity in hopping rates is that paraffin molecules are unaffected by traps and olefin molecule diffusion is hindered.

For traps that are in equilibrium with the applied gas, the fractional filling of traps by olefins is given by the Langmuir adsorption isotherm for a mixed gas system,

$$\theta_{trap} = \frac{p_{ole}\ \exp(\Delta E)}{1 + p_{para} + p_{ole}\ \exp(\Delta E)}, \qquad (11)$$

where p_{ole} and p_{para} are the partial pressures of the olefin and paraffin respectively.

The fractional distance through the membrane may be defined as ξ, where $\xi = 0$ at the upstream face and $\xi = 1$ at the downstream face. As shown in Fig. 4, a "piling up" effect occurs as the trap filling
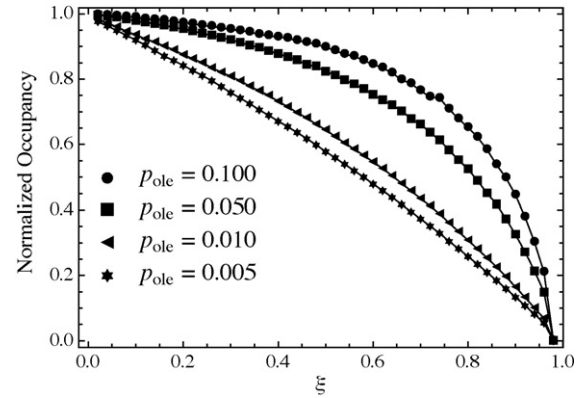
Fig. 4. Trap filling for the KMC model in profile through the membrane are shown as a function of applied pressure at the upstream face. Occupancy values are normalized by the isotherm of Eq. (11) such that 1 is as predicted by the isotherm and 0 is no traps filled. All profiles are time-averaged under steady state conditions for $\rho = 0.2$ and $\Delta E = 9.6$.

profile becomes non-linear. This effect occurs in the limit of low trap loading and high pressures where the effective pressure gradient is roughly linear. In the limit of large trap loading, as seen in Fig. 5, the concentration in ξ approaches the Fickian case with a linear profile.

3.2.1. Sorption and diffusivity of paraffins

Paraffin molecules do not interact with traps and, as a consequence, their overall diffusivity and sorption on trap-containing lattices is affected only by the blocking effect of the olefins. The availability of sites for paraffins through the membrane is controlled by the filling of trap sites by olefins. The concentration along the upstream face is

$$C_{para} = [1 - \rho\theta_{trap}(p_{ole})]\theta(p_{para}). \qquad (12)$$

where θ_{trap} is the fraction of filled traps from Eq. (11) and $\theta(p_{para})$ is the isotherm of Eq. (3) as a function of the partial paraffin pressure.

The diffusivity for paraffins on a square lattice containing mobile obstacles, the olefins bound in traps, cannot be solved exactly. Correlation function analysis reveals the diffusivity to be a product of an obstruction factor, D^*, which is a function of obstacle concentration, c, and the ratio of molecule jump rate to that of the obstacles, γ. The correlation function analysis was performed by van Beijerin and Kutner [35] and and expanded upon by Saxton [36].
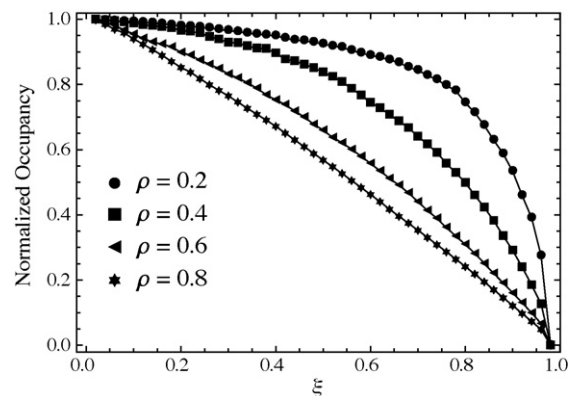
Fig. 5. The KMC model trap fillings in profile through the membrane are shown as a function of trap density on the lattice. The profiles are normalized as detailed in Fig. 4. All profiles are time-averaged under steady state conditions for $p_{ole} = 0.001$ and $\Delta E = 4.8$.

The overall diffusion constant for the molecule diffusing amongst mobile obstacles is

$$D(c, \gamma) = D_{neat}D^*(c, \gamma) = D_{neat}(1 - c)f(c, \gamma). \quad (13)$$

The correlation factor, f, is given by

$$f(c, \gamma) = \frac{\sqrt{A^2 + B^2} - A}{2\gamma(1 - c)f_0}, \quad (14)$$

where

$$A = (1 - \gamma)(1 - c)f_0 + c, \quad (15)$$

$$B = 2\sqrt{\gamma(1 - c)}f_0, \quad (16)$$

and

$$f_0 = \frac{1 - \eta}{1 + (2\gamma - 1)\eta}. \quad (17)$$

The constant η is dependent on the type of lattice; for a square lattice it is equal to $1 - \frac{2}{\pi}$. The ratio of hopping rates γ is given by

$$\gamma = \exp(-\Delta E). \quad (18)$$

The only quantity which is not known analytically in Eqs. (13)–(17) for D^* is the concentration of filled traps, c. To simplify our derivation, we will neglect the inhomogeneity of the filled trap concentration and approximate c as its value at the upstream face

$$c = \rho\theta_{trap}(p_{ole}) \quad (19)$$

For low trap densities and at low pressures Fig. 4 shows that c drops linearly across the membrane. This is the worst case for the approximation – c is overestimated by a factor of two. Fortunately, this low c limit is where D^*, which is largely determined by $(1 - c)$, is close to unity and the value of c is not important. In the high concentration limit where traps strongly effect the diffusivity, the approximation in Eq. (19) becomes increasingly accurate. Although a vacuum at the downstream face is assumed, in the limit of small back pressure, the mean-field approximation becomes more accurate, as well.

In the limit of $\gamma \to \infty$, the percolation threshold is reached at $c \approx 0.41$, above which long range diffusion stops. Below this limit, long-range diffusion is possible but obstructed. The overall diffusivity for paraffins also contains D^* terms due to the blocking effect of paraffins and unbound olefins; however, in the low pressure limit, these terms are close to unity and can be disregarded. The flux, then, of paraffins is produced by combining Eqs. (12) and (13) into Eq. (7) to produce

$$J_{para} = (1 - \rho\theta_{trap})\frac{\theta(p_{para})}{L}\varGamma D^*. \quad (20)$$

Fig. 6 shows the comparison between the analytic model and the full KMC simulation. The KMC data are in agreement with the model at weak binding and low pressure, and although there is some divergence as pressure increases, the trend in paraffin flux is captured over the range of pressures considered.

The approximations that result in the paraffin diffusivity given in Eq. (13) are tested by plotting the transit time as a function of membrane thickness. The transit times for varying thicknesses of the membrane with different applied pressures are shown in Fig. 7. Diffusion is normal for all applied pressures – all transit times are linear in L^2. The ratio of the slopes provides the exact diffusivity experienced by paraffin molecules that leave the membrane through the downstream face. These values from KMC are compared to the value predicted by Eq. (13) in Table 1.

The comparison between the analytical prediction and the KMC data provides a measure of validity for the approximation of c in Eq. (19). Approximating the total concentration of occupied traps by the front end trap filling overestimates the actual filling. In the low pressure cases, the difference between analytical and observed
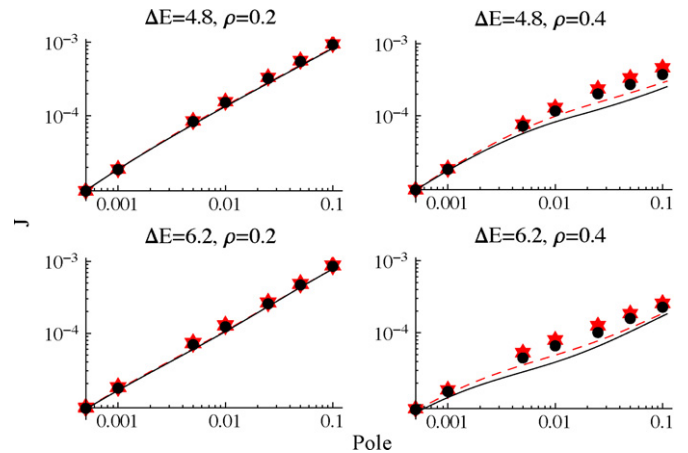
Fig. 6. The flux of paraffins in solid black and olefins in dashed red through the downstream face under different olefin trap depths, ΔE, and trap coverages, ρ, is plotted as a function of partial pressure. Markers – stars for olefins and circles for paraffins – are KMC data and the lines are from Eqs. (20) and (21). (For interpretation of the references to colour in this figure legend, the reader is referred to the web version of the article.)
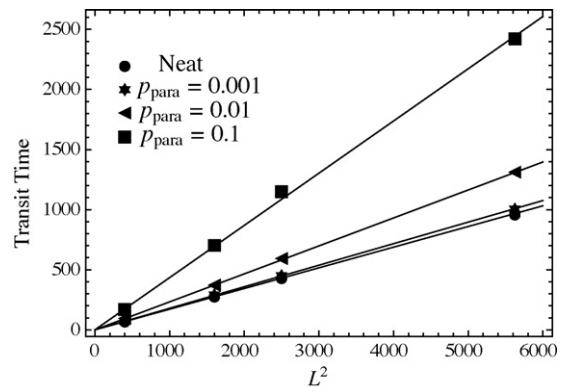
Fig. 7. The average transit times for paraffin molecules in the KMC model are plotted as a function of the square of membrane thickness, L^2 for $\rho = 0.4$ and $\Delta E = 4.8$ at three olefin partial pressures. The neat membrane is shown for comparison. Solid lines are the lines of best fit to the data.

is quite small; however, with increasing pressure the analytical expression underestimates the effective diffusivity by nearly a factor of two. Comparing Table 1 with Fig. 6 provides an explanation for the deviation from the analytical projection in the KMC model. With high pressures, larger fluxes of paraffins are observed than predicted due to the underestimation of the effective diffusivity.

3.2.2. Sorption and diffusivity of olefins

The expression for the permeability of olefin molecules must obey several limiting cases. The net permeability for olefins must converge to that of paraffins in the limit of the trap coverage and/or trap depth going to zero, $\rho \to 0$ and $\Delta E \to 0$, respectively. Similarly, as $\Delta E \to \infty$, the permeability of olefin molecules must return to that of paraffins; this is the case of molecules moving amongst immobile obstacles. To conform with these limiting cases, as $p \to \infty$ or $p \to 0$ the selectivity for olefins over paraffins must return to unity.

Table 1
Comparison of predicted D_{para} to KMC for $\rho = 0.4$ and $\Delta E = 4.8$.

Case	Analytical	KMC
$p_{para} = 0.001$	0.907	0.959
$p_{para} = 0.01$	0.534	0.739
$p_{para} = 0.1$	0.228	0.396

Although molecules may freely diffuse between trap sites and neat sites on the lattice, the steady state statistical behavior may be modeled as two distinct pathways, one containing only neat sites and the other containing only trap sites. The permeability of olefin molecules is thus represented as a sum of terms representing the flux contribution from unbound olefin molecules and that from olefin molecules bound in traps. This model is similar in form to the dual-sorption model [15], which contains a neat membrane term and a term due to the reversible binding at fixed site carriers, the analogue of traps on a lattice.

The permeability from the two modes of transit is

$$P_{ole} = S_{neat}D_{neat} + S_{trap}D_{trap}. \tag{21}$$

The first term in this expression is functionally similar to Eq. (20). The sorption, however, has a slightly different form. Because olefin molecules interact with traps, the maximum amount of unbound olefin molecules is limited to $(1 - \rho)$. In this case, the neat concentration is

$$C_{ole,neat} = (1 - \rho)\theta(p_{ole}). \tag{22}$$

In the limits of low trap coverage, small ρ, Eq. (22) is approximately equal to Eq. (20). The diffusion constant, D_{neat}, is equal to the paraffin case of Eq. (13). As in the paraffin case, additional D^* factors due to blocking effects of paraffins and other unbound olefins are close to unity and may be neglected at low pressure. The neat flux contribution is

$$J_{ole,neat} = \Gamma(1 - \rho)\frac{\theta(p_{ole})}{L}. \tag{23}$$

The second term in Eq. (21) is functionally similar to the neat case. The overall diffusivity is the Einstein–Smoluchowski relation for a homogenous lattice containing only traps which is

$$D_{ole,trap} = D_{neat} \ \exp(-\Delta E). \tag{24}$$

The concentration of filled traps at the front edge is given by Eq. (11) multiplied by ρ, the fraction of trap sites,

$$C_{ole,trap} = \rho\theta_{trap}(p_{ole}). \tag{25}$$

The flux for the trap contribution is obtained from Eqs. (11) and (24) as,

$$J_{ole,trap} = \Gamma\rho\frac{\theta_{trap}(p_{ole})}{L}\exp(-\Delta E). \tag{26}$$

As $p \to \infty$ or $\rho \to 0$, the neat membrane case, this term vanishes.

Fig. 6 shows the agreement between the KMC data and the analytical model of olefin flux. Unlike the paraffin case, the olefin expression does not diverge from observations at large trap concentrations. At high trap concentrations, the term from Eq. (26) dominates.

3.2.3. Selectivity

For olefin/paraffin separation membranes, the parameter that directly measures the membrane's ability to separate the two gases is the selectivity,

$$\alpha = \frac{P_{ole}}{P_{para}} = \frac{J_{ole}}{J_{para}} = \frac{S_{ole}D_{ole}}{S_{para}D_{para}}. \tag{27}$$

The selectivity expression from Eq. (27), when combined with Eqs. (20) and (21), yields the two-term expression

$$\alpha = \frac{S_{ole,neat}D_{ole,neat}}{S_{para}D_{para}} + \frac{S_{ole,trap}D_{ole,trap}}{S_{para}D_{para}}. \tag{28}$$

The first term in this expression, the ratio the permeability of olefin molecules on non-trap sites to the permeability of paraffin molecules, approaches unity as $p \to \infty$. As $p \to 0$, the different sorption expressions from Eqs. (12) and (22) results in this first term approaching $(1 - \rho)$.
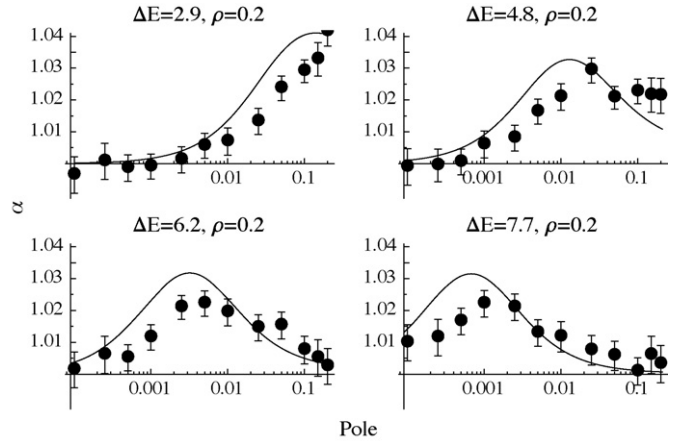

Fig. 8. Selectivity for olefins over paraffins as a function of olefin partial pressure is plotted from KMC data. Solid lines are the analytical expression from Eq. (28).

In the second term, olefin trap sorption is larger than paraffin sorption as $p \to 0$. The olefin trap sorption has a theoretical maximum of ρ, and this is the limiting case as $p \to 0$. With increasing pressure, the denominator [from Eq. (26)] dominates and this term tends toward zero.

The behavior of each of these terms acts in contrast – one rises from $(1 - \rho)$ towards a maximum of unity while another drops from a maximum of ρ toward zero. The rates at which these terms approach the limiting cases are not, however, equal.

The paraffin diffusivity, in the denominator of both terms, depends directly on the olefin trap sorption as shown in Eq. (19). With increasing ΔE and/or pressure, the sorption of olefins on traps becomes larger while the diffusivity of paraffins becomes smaller. This coupling of terms does not lead to a clean analytical derivative for a peak selectivity as a function of pressure in Eq. (28). The overall selectivity as a function of pressure for different trap depths is shown in Fig. 8.

3.2.4. Optimizing selectivity

As discussed in Section 2, a set of macroscopic input parameters are required for our lattice model, including the applied pressure, olefin trap site concentration, and olefin binding energy. From the model, the resulting permeability and selectivity of the membrane can then be determined. The primary focus of this paper is to determine how these properties of interest are dependent upon the input parameters and how they can be optimized within that parameter space.

Some parameter changes have a simple effect. From Eq. (28) it is clear that increasing ρ will increase the olefin trap-diffusion pathway and therefor increase the selectivity. The applied pressure, however, does not lead to a monotonic trend; there is no selectivity of olefins over paraffins in the limits of both high and low pressure.

In the following, we show that there is a peak in selectivity at an optimal applied pressure which is (to first order) directly related to the rate at which olefins leave trap sites. So while it is desirable to maximize both selectivity and the flux of gas through the membrane, we have decomposed these into separate objectives. Given a membrane, we show how to set the applied pressure to maximize selectivity. Then, the membrane parameters can be adjusted to maximize flux while maintaing optimal selectivity (by, for example, reducing the binding of olefins to traps).

The two-term expression for selectivity in Eq. (28) may be simplified in order to find a derivative that gives a reasonable prediction of the peak position in pressure. In the first term, the ratio $\frac{D_{ole,neat}}{D_{para}}$ is equal to unity and may be ignored. This first term may

now be represented as

$$\frac{S_{ole,neat}}{S_{para}} = \frac{p_{ole}(1-\rho)}{p_{para} - \frac{p_{para}p_{ole}\rho}{\gamma+\gamma p_{ole}+p_{ole}}}, \tag{29}$$

where $\gamma = \exp(-\Delta E)$ is the same as in Eq. (18).

The second term is more complex; however, it may be simplified. From Eq. (13), $f(c, \gamma)$ is close to unity and slow to change with pressure, so it may be ignored. The ratio of diffusivities reduces to

$$\frac{D_{ole,trap}}{D_{para}} \approx \frac{\gamma}{1 - \frac{p_{ole}\rho}{\gamma+\gamma p_{ole}+p_{ole}}}, \tag{30}$$

if $f(c, \gamma)$ is disregarded. Similarly, the sorption ratio is

$$\frac{S_{ole,trap}}{S_{para}} = \frac{\rho(1 + p_{para} + p_{ole})p_{ole}}{[\gamma + p_{ole}(\gamma + 1 - \rho)]p_{para}}. \tag{31}$$

These equations simplify by considering the case where $p_{ole} = p_{para}$. Putting Eq. (29) plus the product of Eqs. (30) and (31) together, taking the derivative, and setting it to zero yields the pressure for which selectivity is maximized,

$$p_{max\alpha} = \frac{2(\gamma^2 + \gamma\rho)}{\rho - \gamma - (\gamma - \rho)^2}. \tag{32}$$

The full selectivity expression for Eq. (28) is plotted with KMC data in Fig. 8. Peaks in selectivity from the KMC simulations are accurately reproduced with the analytical model; the actual magnitude of selectivity, however, is somewhat overestimated.

In Fig. 8, a clear trend is present: the peak of selectivity occurs at large pressures for weak binding and at small pressures for strong binding. With trap depth and pressure there is a tradeoff. High pressures and trap depths increase olefin sorption and drive down paraffin diffusivity. However, from Eq. (26), as $p \to \infty$ and $\Delta E \to \infty$, the olefin trap permeability – and consequently the second term of Eq. (28) – is driven to zero. The predicted pressure at which the peak of selectivity occurs is plotted against KMC data in Fig. 9. The KMC data follows the analytical model quite closely.

As a first approximation to Eq. (32), the maximum of selectivity may be reduced to

$$p_{max\alpha} \approx 2\gamma. \tag{33}$$

The implication of Eq. (33) is that selectivity is maximized at the point when the applied pressure is equal to the Arrhenius factor for escaping a trap site. At this point, molecules are entering the lattice at the same rate that trapped molecules are leaving traps.

Two limiting cases are apparent. In the limit where $\gamma \sim \rho$, the squared term in the denominator of Eq. (32) can be ignored and the
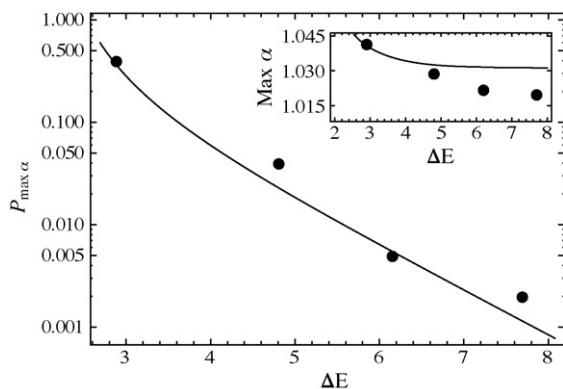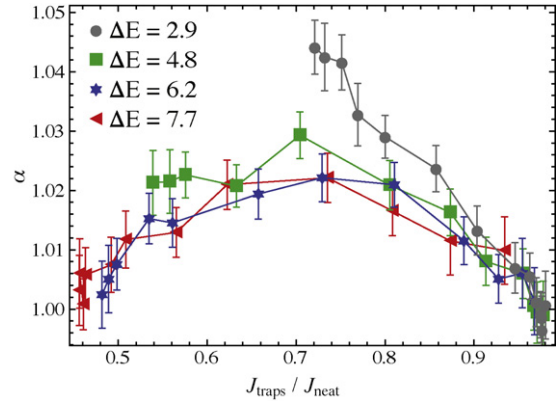
Fig. 10. The selectivity data from Fig. 8 is plotted against the olefin flux at that pressure normalized by the neat membrane flux from Eq. (7). The x-axis is the ratio of olefin flux for membranes with traps to the neat membrane flux at the same pressure.

entire expression is reduced via Taylor expansion to

$$p_{max\,\alpha} \approx 2\gamma \left(1 + \frac{2\gamma}{\rho}\right). \tag{34}$$

In the weak binding limit, the second term explains the curve observed in Fig. 9. In the limit of $\gamma \ll \rho$, however, the squared term behaves simply like ρ^2. Considering this limit, Eq. (32) reduces to

$$p_{max\,\alpha} \approx 2\gamma \; \exp(-\rho). \tag{35}$$

Eq. (34) contains an additional term that become significant as γ approaches the same order of ρ. This correction term shifts the peak of selectivity to an applied pressure that is slightly larger than the escape rate from the traps.

Substituting Eq. (34) into Eq. (27) gives the magnitude of selectivity at the optimal pressure for each trap binding energy. As shown inset in Fig. 9, the actual magnitude of selectivity at the optimal pressure for a given binding energy is not constant. Both KMC data and the analytical model indicate that more selectivity is possible for weaker binding. Our model indicates that when the pressure is optimal for the binding energy, weaker binding is preferable due to the larger resulting selectivity.

3.2.5. Comparison to neat membrane

Maximizing selectivity by increasing the concentration of traps and applying the optimum pressure may not be ideal for producing a physical membrane. Traps, by definition, slow the diffusion of molecules. An ideal membrane maximizes both selectivity and the flux of olefins. At large trap depths, the benefit of the large selectivity is offset but the slow transit of olefin molecules.

The selectivity data at various pressures for $\rho = 0.2$ is plotted on the y-axis of Fig. 10 while the x-axis is the olefin flux for the trap-containing membrane divided by the neat membrane flux at the same pressure. The common position of the maxima demonstrates that increasing the trap depth does not affect the relative permeability at peak selectivity.

In the regime of low applied pressures, the sorption profile is roughly linear – double the pressure means roughly double the resulting flux. Given that there is the same flux penalty for introducing trap sites regardless of ΔE at the pressure of peak selectivity, in absolute terms it is most sensible to design membranes with weak binding trap sites. These membranes maximize selectivity at high pressures, and, in absolute terms, the flux of olefins is maximized as well.

Fig. 9. The peak of selectivity from KMC data is plotted against Eq. (32) for $\rho = 0.2$. Inset is the analytical magnitude of selectivity at $p_{max\,\alpha}$ for each ΔE along with the corresponding KMC data.

4. Conclusions

We have presented a lattice model of nanoparticle-containing membranes that identifies parameters to enhance olefin/paraffin separation. Olefins bind tightly to nanoparticles due to a d–π^* interaction that is unavailable to paraffins. In steady state, a larger flux of olefins is noted as a function of applied pressure, nanoparticle binding energy, and area fraction of nanoparticle binding sites in the membrane. We show, both numerically and analytically, how the selectivity and permeability of the membrane depend upon these parameters.

Our model demonstrates that change in permeability of paraffins is the result of both sorptive and diffusive effects. The sorption of paraffins is driven downward due to the lack of available sites as traps begin to fill with pressure. The diffusivity of paraffins is analogous to the case of tracer diffusion in an archipelago of mobile obstacles. Long-range diffusion is obstructed but possible as long as the obstacles are mobile and diffusion is normal over long distances. Overall olefin permeability is the statistical average of contributions from olefin molecules in neat and trap regions. Neat olefin diffusivity is exactly that of paraffins – obstructed by slower moving obstacles. Trap olefin diffusivity, however, is slowed by the energy of binding to traps the and resulting lower Arrhenius diffusion rate. The lowered diffusivity of olefin molecules is offset by the increase in sorption due to the filling of the traps.

We show that the balance between sorption and diffusivity for olefins is not perfectly offsetting and that selectivity is the result. The selectivity of olefins is maximized when the applied pressure results in a rate molecules entering the membrane that is comparable to the rate olefins leave traps. When the optimum pressure is applied, the selectivity is constant for strong binding and increases for weaker binding. Thus, weaker binding traps offer higher selectivity at the optimal pressure.

From this model, trends of selectivity in physical membranes may be predicted. Increasing the fraction of olefin-binding sites (concentration of nanoparticles) in the membrane will increase the selectivity. The optimum pressure to maximize selectivity is directly related to the binding energy of olefins onto the traps. If the binding of olefins is reduced, then the applied pressure must be higher to maximize selectivity. The maximum of selectivity at the optimal pressure is constant in the strong binding regime and becomes larger in the weak binding regime.

Starting from five macroscopic parameters – sorption, diffusivity, binding energy, pressure, and area fraction of nanoparticles – it is possible to predict the selective behavior of a membrane and identify trends as these parameters are adjusted. The optimization criteria can now be tested experimentally to verify our design principles for making better separation membranes.

References

[1] T. Ren, M.K. Patel, K. Blok, Energy 33 (2008) 817.
[2] R.B. Eldridge, Ind. Eng. Chem. Res. 32 (1993) 2208.
[3] C. Staudt-Bickel, W.J. Koros, J. Membr. Sci. 170 (2000) 205.
[4] J.G. Wijmans, R.W. Baker, in: Y. Yampolskii, I. Pinnau, B. Freeman (Eds.), Materials Science of Membranes for Gas and Vapor Separation, Wiley, 2006, pp. 159–190 (Chapter 5).
[5] W.J. Koros, R. Mahajan, J. Membr. Sci. 175 (2000) 181.
[6] P. Pandey, R.S. Chauhan, Prog. Polym. Sci. 26 (2001) 853.
[7] E. Smit, M.H.V. Mulder, C.A. Smolders, H. Karrenbeld, J. van Eerden, D. Feil, J. Membr. Sci. 73 (1992) 247.
[8] E. Tocci, D. Hoffman, D. Paul, N. Russo, E. Drioli, Polymer 42 (2001) 521.
[9] E. Tocci, E. Bellacchio, N. Russo, E. Drioli, J. Membr. Sci. 206 (2002) 289.
[10] M. Meunier, J. Chem. Phys. 123 (2005) 134906.
[11] S.Y. Lim, T.T. Tsotsis, J. Chem. Phys. 119 (2003) 496.
[12] J. ichiro Hayashi, H. Mizuta, M. Yamamoto, K. Kusakabe, S. Morooka, Ind. Eng. Chem. Res. 35 (1996) 4176.
[13] S.S. Chan, T.-S. Chung, Y. Liu, R. Wong, J. Membr. Sci. 218 (2003) 235.
[14] R.L. Burns, W.J. Koros, J. Membr. Sci. 211 (2003) 299.
[15] Y.S. Kang, J.H. Kim, J. Won, H.S. Kim, in: Y. Yampolskii, I. Pinnau, B. Freeman (Eds.), Materials Science of Membranes for Gas and Vapor Separation, Wiley, 2006, pp. 391–410 (Chapter 16).
[16] W.S. Ho, D.C. Dalrymple, J. Membr. Sci. 91 (1994) 13.
[17] I. Pinnau, L.G. Toy, J. Membr. Sci. 184 (2001) 39.
[18] A. Morisato, Z. He, I. Pinnau, T.C. Merkel, Desalination 145 (2002) 347.
[19] Y.S. Park, J. Won, Y.S. Kang, J. Membr. Sci. 183 (2001) 163.
[20] T. Yamaguchi, C. Baertsch, C.A. Koval, R.D. Noble, C.N. Bowman, J. Membr. Sci. 117 (1996) 151.
[21] H.S. Kim, J.H. Ryu, H. Kim, B.S. Ahn, Y.S. Kang, Chem. Commun. 14 (2000) 1261.
[22] Y.S. Kang, S.W. Kang, H. Kim, J.H. Kim, J. Won, C.K. Kim, K. Char, Adv. Mater. 19 (2007) 475.
[23] S.W. Kang, D.H. Lee, J.H. Park, K. Char, J.H. Kim, J. Won, Y.S. Kang, J. Membr. Sci. 322 (2008) 281.
[24] S.H. Mun, S.W. Kang, J.-S. Cho, S.-K. Koh, Y.S. Kang, J. Membr. Sci. 332 (2009) 1.
[25] S.W. Kang, K. Char, Y.S. Kang, Chem. Mater. 20 (2008) 1308.
[26] M. Becker, J. Brock, H. Cai, D. Henneke, J. Keto, J. Lee, W. Nichols, H. Glicksman, Nanostruct. Mater. 10 (1998) 853.
[27] H. Cai, N. Chaudhary, J. Lee, M. Becker, J.R. Brock, J. Keto, J. Aerosol Sci. 29 (1998) 627.
[28] I. Gallardo, K. Hoffman, J. Keto, Appl. Phys. A 94 (2009) 65.
[29] H. Han, Y. Feng, Z. Li, H. Xu, Appl. Phys. Lett. 82 (2008) 023116.
[30] H. Zeng, S. Sun, J. Li, Z.L. Wang, J.P. Liu, Appl. Phys. Lett. 85 (2004) 792.
[31] W. Tang, G. Henkelman, J. Chem. Phys. 130 (2009) 194504.
[32] N.S. Froemming, G. Henkelman, J. Chem. Phys. 131 (2009) 234103.
[33] A.F. Voter, in: K.E. Suckafus, E.A. Kotomin, B.P. Uberuaga (Eds.), Radiation Effects in Solids, Springer, NATO Publishing Unit, Dordrecht, The Netherlands, 2006, pp. 1–24.
[34] S. Chandrasekhar, Rev. Mod. Phys. 15 (1943) 1.
[35] H. van Beijeren, R. Kutner, Phys. Rev. Lett. 55 (1985) 238.
[36] M.J. Saxton, Biophys. J. 52 (1987) 989.